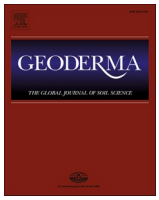
Geoderma 474 (2026) 118060



Contents lists available at ScienceDirect

Geoderma

journal homepage: www.elsevier.com/locate/geoderma



Nonlinear loss of recalcitrant organic carbon in saltmarsh sediments following *Spartina alterniflora* eradication: Evidence from microbial metabolic shifts

Hui Wu [a,b,c], Meiqing Lu [d], Dan Yu [e], Wenhong Xu [a], Mengru Li [a], Shiyao Chen [a], Zeyang Lu [f], Fenfang Wang [g], Nengwang Chen [a,b,c,*]

[a] Fujian Provincial Key Laboratory for Coastal Ecology and Environmental Studies, College of the Environment and Ecology, Xiamen University, Xiamen 361102, China
[b] State Key Laboratory of Marine Environmental Science, Xiamen University, Xiamen 361102, China
[c] National Field Observation and Research Station (Fujian Taiwan Strait) for Marine Ecosystem, Xiamen University, Zhangzhou 363000, Fujian, China
[d] CUG-HKU Joint Centre for Coastal Groundwater and Ecosystem, School of Environmental Studies, China University of Geosciences, Wuhan 430078, China
[e] Key Laboratory of Global Change and Marine-Atmospheric Chemistry, Third Institute of Oceanography, Ministry of Natural Resources, Xiamen 360115, China
[f] Fujian Provincial Key Lab of Coastal Basin Environment, Fujian Polytechnic Normal University, Fuqing 350300, China
[g] Polar and Marine Research Institute, College of Harbor and Coastal Engineering, Jimei University, Xiamen 361021, China

ARTICLE INFO

Handling Editor: Dr Cornelia Rumpel

Keywords:
Mangrove wetland
Blue carbon
Ecological restoration
Sediment organic carbon
Recalcitrant organic carbon
Microbial carbon metabolism

ABSTRACT

Large-scale eradication of the invasive *Spartina alterniflora* on China's coasts is implemented to restore wetland ecosystems, yet it introduces a critical yet overlooked environmental trade-off: massive plant residue input may destabilize sediment organic carbon (SOC), the core part of coastal blue carbon. While carbon loss from biomass removal is recognized, the impact on the recalcitrant organic carbon (ROC) pool remains unknown. Here, we conducted field measurement in a subtropical mangrove wetland in Southeast China with a 60-day incubation experiment across five plant residue-addition gradients, using ^{13}C isotope tracing and metagenomics to quantify ROC loss and to explore its microbial mechanisms. Field observations post-eradication showed the ROC to SOC ratio decreased by 11%–19%. Incubation experiments provided the direct evidence of nonlinear, dose-dependent ROC loss, with low-dose inputs inducing disproportionately greater loss. All residue addition treatments showed net ROC loss (12%–383%), whereas only the lowest addition (0.5 kg dry residue m^{-2}) caused net SOC loss (63 %) compared with control group. Metagenomic analysis further showed that the lower-dose treatment (1 kg m^{-2}) was enriched in MAGs with broader predicted capacities for complex-carbon utilization, whereas the high-dose treatment (4 kg m^{-2}) showed greater potential for plant-derived carbohydrate utilization. This study establishes a mechanistic link between invasive plant eradication and nonlinear ROC loss, providing a critical perspective for optimizing coastal blue carbon management during ecological restoration.

1. Introduction

Coastal wetlands, including mangroves and saltmarshes, are globally important blue carbon ecosystems (Macreadie et al., 2021). Their high primary productivity combined with the anaerobic conditions, promotes substantial burial and storage of organic carbon in sediments, making them significant carbon sinks (Alongi, 2022; Sun et al., 2023). However, in recent years, biological invasions—particularly by the alien species *Spartina alterniflora* (*S. alterniflora*)—have profoundly affected the ecological structure and functioning of coastal wetlands in China. With ongoing eradication efforts and subsequent maintenance, China has restored over 60,000 ha of *S. alterniflora*-invaded wetlands (Li et al., 2022a; Mao et al., 2019), removing more than 7.5×10^5 t of above-ground biomass (dry weight) (Xie, 2019). This large-scale removal is thought to have substantially reduced blue carbon stocks (Qi et al., 2024). Understanding and potentially managing the factors that influence sediment carbon sequestration in response to *S. alterniflora* residues is therefore of critical importance.

* Corresponding author.
E-mail addresses: wuhui@stu.xmu.edu.cn (H. Wu), lumeiqing66@163.com (M. Lu), danyu2021@xmu.edu.cn (D. Yu), xuwenhong@stu.xmu.edu.cn (W. Xu), limengru@stu.xmu.edu.cn (M. Li), shiyaochen@stu.xmu.edu.cn (S. Chen), zeyanglu@stu.xmu.edu.cn (Z. Lu), ffwang@jmu.edu.cn (F. Wang), nwchen@xmu.edu.cn (N. Chen).

https://doi.org/10.1016/j.geoderma.2026.118060
Received 8 December 2025; Received in revised form 19 September 2026; Accepted 21 September 2026
Available online 25 September 2026
0016-7061/© 2026 The Author(s). Published by Elsevier B.V. This is an open access article under the CC BY license (http://creativecommons.org/licenses/by/4.0/).

Although large-scale eradication projects have been implemented, empirical evidence regarding their impact on sediment carbon pools remains contradictory. Some studies report substantial inputs of plant-derived carbon have the potential to increase SOC storage. For instance, observations in the Yellow River Estuary reported increased SOC one year after *S. alterniflora* removal (Song et al., 2024). However, a study in the Chongming Dongtan wetland in the Yangtze River Estuary found SOC decreased following eradication (Wang et al., 2025a). These differences may be due to the "priming effect" (Jian et al., 2020), which can be very sensitive to the amount of added carbon (Mendoza et al., 2022; Li et al., 2024). Importantly, most studies focus on total SOC, but the fate of recalcitrant organic carbon (ROC), which is the main form of long-term carbon storage, under different residue amounts is still unclear. Therefore, it is unknown whether there is a "tipping point" in residue input that shifts sediments from storing carbon to losing ROC. As a result, it remains unclear whether *S. alterniflora* residues should be buried in situ or transported off-site for treatment, and if buried locally, what amount of residue input would best enhance SOC storage or minimize its destabilization.

ROC contains highly aromatic or structurally complex compounds that resist rapid microbial decomposition, making it the principal component of long-term carbon storage in wetland sediments (Yang et al., 2013). As a result, any change in ROC directly determines whether a restored wetland can maintain its function as a carbon sink (Cheng et al., 2007; Liu et al., 2025a). The introduction of fresh organic carbon into sediments may cause a priming effect (PE) (Kuzyakov, 2010), whereby the decomposition of native SOC is either stimulated (positive PE) or suppressed (negative PE). Positive PE has been reported when residue inputs enhance microbial activity and accelerate native organic matter mineralization (Bernard et al., 2022; Fontaine et al., 2007), whereas residues with high C/N ratios may induce negative PE due to microbial competition for electron acceptors or the inhibition of extracellular enzymes (Craig et al., 2022; Kuzyakov et al., 2000). Previous studies have also shown that the intensity of PE does not increase proportionally with elevated labile organic carbon inputs, suggesting that microbial responses to fresh carbon may shift with substrate availability (Paterson and Sim, 2013). When fresh carbon supply is limited, microbial communities may shift toward taxa with oligotrophic traits, such as members of Acidobacteriota and Chloroflexota, which are generally better adapted to resource-limited conditions (Li et al., 2022b; Yu et al., 2025). Under such conditions, microorganisms may broaden their substrate use and increase investment in extracellular enzymes to access more complex native organic matter (Fontaine et al., 2007; Fang et al., 2018). In contrast, when readily available substrates are abundant, fast-growing copiotrophic microorganisms, such as members of Proteobacteria and Bacillota, can preferentially exploit these inputs, potentially reducing their relative dependence on native recalcitrant carbon (Garcia-Pausas and Paterson, 2011; Bernard et al., 2022). Such a shift in microbial carbon-acquisition strategy provides a plausible explanation for why priming responses may vary nonlinearly with the amount of fresh organic carbon supplied. However, whether different amounts of *S. alterniflora* residues induce such contrasting microbial strategies, and how these shifts are associated with the destabilization of sediment ROC, remains unknown. Unraveling these dose-dependent microbial mechanisms is critical to understanding why massive residue inputs might counterintuitively accelerate the loss of the wetland's most stable carbon fraction.

To address these knowledge gaps, we combined field observations in a subtropical mangrove wetland with a 60-day incubation experiment using ^{13}C stable isotope tracing and metagenomic analysis across a range of *S. alterniflora* residue additions. We focused on two main questions: (1) How does the amount of residue added affect the balance between *S. alterniflora* residue carbon accumulation and the loss of ROC? and (2) What microbial processes drive ROC loss under low versus high residue inputs? We hypothesize that residue input does not always increase total SOC, but can cause nonlinear, dose-dependent carbon accumulation or loss, particularly affecting ROC.

2. Materials and methods

2.1. Field study

The study area is located in the Zhangjiang Estuary National Mangrove Nature Reserve, Zhangzhou, Fujian Province, China (117°24′07″–117°30′00″E, 23°53′45″–23°56′00″N) (Gao et al., 2018). The reserve covers a total area of 2,360 hm^2, with dominant mangrove species including *Kandelia obovata*, *Avicennia marina*, and *Aegiceras corniculatum*. Since the 1990s, the mudflats of this region have been invaded by *S. alterniflora*, which competed strongly with native mangroves (Zhu et al., 2019). By 2016, the invaded area had exceeded that of the mangroves, and by 2022, the invasion expanded to 132.12 hm^2 (Huang et al., 2022). In late October 2022, a one-month restoration project was launched (Zhu et al., 2024, Zhu et al., 2025), during which the invasive *S. alterniflora* was effectively removed through a combination of mowing and ploughing.

Sediment samples were collected from three stations (S1–S3; Fig. S1). Pre-eradication samples (n = 3 per station) were obtained in October 2019 (S1), November 2020 (S2), and August 2022 (S3), while post-eradication samples were collected in August 2023 (S1, S2, S3). Before eradication, all sampling sites were characterized by dense monospecific stands of *S. alterniflora*, with no intermixing with mangroves or other vegetation. Following eradication, all sites were characterized by unvegetated mudflat conditions (Fig. S1). The sampling stations were located approximately 10–30 m from the nearest tidal creek. During low tide, surface sediments from the upper 5 cm, representing the sediment layer most directly exposed to vegetation removal, residue incorporation, and subsequent biogeochemical disturbance, were collected using a hand shovel, placed in sterile polyethylene bags, and immediately stored in insulated containers with dry ice before being transported to the laboratory within 24 h for subsequent analyses of SOC, ROC, and $\delta^{13}C$. Sediments were freeze-dried and stored at −80 ℃ until further processing.

2.2. Controlled sediment experiments

For laboratory incubation, sediments were collected from S3 in August 2023 using Plexiglas corers (120 mm diameter × 500 mm length) from three profiles, pooled, and homogenized. Plant residues and stones were removed by sieving through a 2 mm mesh. Sediment slurries were prepared by mixing sediments with in situ seawater, which had been filtered through 0.7 μm glass-fiber filters (Whatman GF/F, USA), at a ratio of 1:1 (m/v). Whole plants of *S. alterniflora* were harvested from quadrats (1 m × 1 m). Adhering sediments were removed using a high-pressure water jet, followed by a second cleaning with Milli-Q water. The plants were subsequently oven-dried at 65 ℃, cut into small fragments (< 1 mm), and finely ground using a ball-mill homogenizer (JXFSTPRP, Jingxin, China).

The incubation experiment used *S. alterniflora* (a C4 plant) residues mixed with sediments collected from a mangrove (C3) wetland that had previously been invaded by this species. Considering that the aboveground biomass of *S. alterniflora* in our region ranges from 0.24 to 3.69 kg dry m^{-2} (Huang et al., 2022), five residue-addition levels were established: 0, 0.5, 1, 2, and 4 kg dry m^{-2}. Based on the sediment bulk density of 0.8 g cm^{-3} and the ploughing depth of 0.4 m, these levels corresponded to the addition of 0, 0.25, 0.5, 1, and 2 g of *S. alterniflora* dry residues to approximately 400 g of slurry (equivalent to 160 g dry sediment). For each treatment, the five doses of *S. alterniflora* residue (C content: 37.0 % ± 0.25; $\delta^{13}C$: −14.48 ‰ ± 0.12) were thoroughly mixed with 400 g of slurry (C content: 1.28 % ± 0.13; $\delta^{13}C$: −25.31 ‰ ± 0.05) and transferred to 1 L sealed incubation bottles. Samples were incubated under anoxic, dark conditions at in situ temperature (30 ℃) for 60 days.

Destructive sampling was performed on days 7, 30, and 60, with

three replicates for each treatment. Treatments with 0 kg m^{-2} (CK, control), 1 kg m^{-2} (L, low dose), and 4 kg m^{-2} (H, high dose) were selected for metagenomic sequencing to contrast microbial responses across no-input, environmentally representative low-input, and high-input conditions. The 0.5 kg m^{-2} treatment was included primarily to resolve the full dose–response of sediment carbon pools and represents an extreme low residue-input scenario. SOC, ROC and isotope were measured only at the end of the incubation because they represent relatively stable sediment carbon pools. CO_2 and CH_4 production during the incubation showed that microbial decomposition reached a steady state after approximately 45 days (Fig. S2). Therefore, end-point measurements minimized short-term variability and better captured the net changes in sediment carbon pools resulting from the degradation of the added plant residues.

2.3. SOC, ROC and stable-isotope analyses

Sediment pretreatment and analytical methods followed (Lu et al., 2023). ROC was determined using the acid hydrolysis method (Cheng et al., 2007). In this study, ROC was operationally defined as the SOC fraction remaining after acid hydrolysis, representing a chemically resistant fraction of bulk SOC rather than an intrinsically inert carbon pool. Freeze-dried sediment samples were cleaned of visible plant and animal residues, and 1 g of sediment was placed into an Erlenmeyer flask with 20 mL of 6 mol L^{-1} HCl. The samples were heated at 116 °C under reflux on a digestion block for 18 h. After cooling, the samples were centrifuged, and the supernatant was discarded. The sediment was rinsed with Milli-Q water until neutral, then freeze-dried and ground. SOC and ROC contents were measured using an elemental analyzer (Vario EL III, Elementar, Germany), and $\delta^{13}C$ values were measured using an isotope ratio mass spectrometer (MAT 253, Thermo Fisher Scientific, USA).

The contribution proportion (f) of *S. alterniflora* residues to SOC or ROC after incubation was calculated using a binary mixing model (Sauvadet et al., 2018).

$$f = (\delta^{13}C_{sample}\text{-}\delta^{13}C_{raw})/(\delta^{13}C_{SA}\text{-}\delta^{13}C_{raw}) \times 100\% \quad (1)$$

In the equation, *f* represents the proportion (%) of SOC or ROC derived from *S. alterniflora* residues. $\delta^{13}C_{sample}$ is the $\delta^{13}C$ value (‰) of SOC or ROC in sediments after incubation, $\delta^{13}C_{raw}$ is the $\delta^{13}C$ value of SOC or ROC in the initial sediments used for incubation (δ^{13}C-SOC = -25.3 ‰, δ^{13}C-ROC = -24.8 ‰), and $\delta^{13}C_{SA}$ is the $\delta^{13}C$ value of the added plant residues ($\delta^{13}C_{SA}$ = -14.48 ‰ in this study).

The absolute amount of *S. alterniflora*-derived carbon incorporated into the sediments was calculated using Eq. (2).

$$SAderived = f \times C_{sample} \quad (2)$$

In the equation, $SA_{derived}$ represents the amount of carbon (mg) in SOC or ROC derived from *S. alterniflora* residues at the end of incubation, while C_{sample} denotes the SOC or ROC content (mg) in sediments of each treatment after incubation.

To evaluate the dose effect of plant residues input on SOC and ROC, we calculated the change in SOC or ROC per unit of residues added (ΔC). Specifically, the difference in SOC or ROC between each treatment and the control (0 kg m^{-2}) was divided by the amount of residues added Eq. (3).

$$\Delta C = (C_{sample} - C_{ck})/(C_{residues}) \times 100\% \quad (3)$$

In the equations, C_{CK} denotes the SOC or ROC content (mg) in the control treatment without residue addition. $C_{residues}$ represents the added amount of plant carbon in each treatment. Accordingly, ΔC > 0 indicates a net gain in the corresponding sediment carbon pool relative to the control per unit of residue C added, whereas ΔC < 0 indicates a net loss. In particular, a negative ΔC indicates that the loss of pre-existing sediment carbon exceeded the amount of residue-derived carbon retained in that carbon pool. In this study, the amount of $C_{residues}$ in the five experimental treatments was 0, 93.7, 187.3, 374.6, and 749.2 mg, respectively.

2.4. DNA extraction and shotgun metagenomic sequencing

DNA was extracted using the HiPure Soil DNA Kit B (Magen, China). DNA quality was checked with a NanoDrop (Thermo Scientific, USA), and concentration was determined using a Qubit 4 Fluorometer (Thermo Scientific, USA). DNA was fragmented to 300–350 bp with a Covaris S220 ultrasonicator, followed by end repair, adaptor ligation, PCR amplification, purification, and library quality assessment. Qualified libraries were sequenced on the MGIseq-T7 platform (PE150), generating an average of 50 Gbp paired-end reads per sample (Table S1).

Metagenomic data processing generally followed Fan et al. (2024) and Wu et al. (2026). Raw reads were converted to FASTQ format, and adaptor sequences and low-quality reads were removed using cutadapt (v1.9.1) (Martin, 2011). Clean reads were assembled with MEGAHIT (v1.1.3) (Li et al., 2015), and coding sequences were predicted using Prodigal (v3.02) (Hyatt et al., 2010). A non-redundant unigene catalog was constructed with MMseqs2 using 95 % sequence identity and 95 % coverage thresholds (Steinegger and Söding, 2017). Gene abundance was estimated by mapping clean reads to the unigene catalog using SoapAligner (v2.21) (Li et al., 2009). Predicted proteins were annotated against the KEGG Genes and NCBI NR databases using DIAMOND (v0.8.15.77), with an e-value cutoff of 1×10^{-5} and a minimum identity of 30 %, retaining the best hit (Buchfink et al., 2015). Carbohydrate-active enzymes (CAZymes) were identified using the CAZy database and annotated with HMMER against the dbCAN3 HMM profiles (Zheng et al., 2023). Relative abundances of functional genes and CAZy families were then calculated to characterize community-level metabolic potential and carbohydrate utilization capacity.

Metagenome binning was conducted with metaWRAP (v1.3.2) (Uritskiy et al., 2018), integrating MetaBAT2 (v2.12.1) (Kang et al., 2019), MaxBin2 (v2.2.6) (Wu et al., 2016), and CONCOCT (v1.1.0) (Alneberg et al., 2014). Bins were refined using the metaWRAP refinement module and evaluated with CheckM2 (v1.1.0) (Chklovski et al., 2023). MAGs with completeness > 50 % and contamination < 10 % were retained, yielding 414 MAGs. Dereplication with dRep (v3.6.2) at a 95 % ANI threshold produced 261 unique clusters (Olm et al., 2017). MAG relative abundance was calculated using CoverM (v0.7.0) (Wang et al., 2024). At the genome-resolved level, taxonomic classification of individual MAGs was performed using GTDB-Tk (v2.5.1) (Chaumeil et al., 2020), and their predicted complex carbon degradation capacities were annotated using METABOLIC (v4.0) (Zhou et al., 2022). This analysis identified 211 MAGs containing predicted functions related to complex-carbon degradation, and the 40 most abundant MAGs were selected for subsequent analysis (Fig. S5; Tables S2 and S3).

2.5. Data analysis

Bar charts present the mean values and standard errors (n = 3), illustrating the differences in carbon fractions and sources pre- and post-*S. alterniflora* residues input in field and laboratory experiments. Figures were generated using Origin 2025 (OriginLab Corporation). Microbial annotation and alignment results were analyzed in R v4.3.3 (R Core Team, 2023). Based on species-level taxa data, the Shannon index was calculated using the "diversity" function in the vegan package to assess α-diversity. The "vegdist" function with the Bray–Curtis method was used for NMDS analysis, visualizing sample similarities and differences across treatments and incubation times. PERMANOVA was performed using the "adonis2" function to test community variation. Grouped hierarchical heatmaps were generated with the pheatmap package to visualize sample similarities and dissimilarities.

3. Results

3.1. Changes in field SOC pools between pre- and post-eradication

We found no significant differences in SOC and ROC contents between pre- and post- *S. alterniflora* eradication (Fig. 1a, b). Because the pre-eradication samples were collected in different years, natural interannual variability cannot be fully excluded. Therefore, these field observations should be regarded as contextual evidence of changes in surface sediment carbon-pool composition rather than as a stand-alone causal test of the eradication effect. Despite similar absolute concentrations, the composition of the sediment organic carbon pool shifted after eradication. The proportion of ROC in SOC decreased by 11–19 % (Fig. 1c). The $\delta^{13}C$ data indicate that the increase in SOC was largely derived from *S. alterniflora* inputs (10–22 %; Fig. 1d), which contain both labile and recalcitrant components.

3.2. Changes of SOC and ROC with residues addition

To evaluate the effects of different residue addition levels, the change in sediment carbon per unit of added residues (ΔC) was calculated by comparing the SOC or ROC content in each treatment to the control (0 kg m^{-2}) and normalizing it by the amount of residue carbon added, as shown in Equation (3). In other words, ΔC represents the amount of carbon gained or lost in the sediment relative to the residue input (Fig. 2). Only the lowest residue addition (0.5 kg m^{-2}) resulted in a negative ΔC_{SOC} (−63%), indicating that carbon losses exceeded the amount of residue-derived carbon retained in the SOC pool. In contrast, ΔC_{SOC} was positive at the higher residue additions (Fig. 2a, S3). A distinctly different pattern was observed for ROC (Fig. 2b, S2b). ΔC_{ROC} remained negative across all residue-addition treatments (−12% to −383%), with the greatest input-normalized ROC loss occurring at 0.5 kg m^{-2}. Thus, although residue addition destabilized pre-existing ROC across the entire addition gradient, only at the lowest residue input did this loss exceed the accumulation of added carbon sufficiently to produce a net loss of the total SOC pool. SOC derived from *S. alterniflora* increased by 68–126% across all addition treatments, with the largest increase in the low-dose treatment (Fig. 2c, S2c). ROC derived from *S. alterniflora* increased by 12–28% (Fig. 2d, S2d).

3.3. Microbial community structure dynamics following residues addition

S. alterniflora residues addition increased both the diversity and abundance of microbial communities (Fig. 3a, b). Community composition varied across residues doses and sampling times (Fig. 3c), with the H treatment harboring the largest number of unique taxa (Fig. 3d). At the phylum level, compared to CK, residues addition increased the relative abundances of Bacillota (formerly Firmicutes), Bacteroidota, Fibrobacterota, Euryarchaeota, and Spirochaetota, while decreasing those of Pseudomonadota, Gemmatimonadota, Acidobacteriota, Verrucomicrobiota, Planctomycetota, Ignavibacteriota, Chloroflexota, and Myxococcota (Fig. 3e; Fig. S3). For fungi, residues addition increased the abundances of Ascomycota and Chytridiomycota, whereas a decline in Basidiomycota was observed exclusively in the H treatment (Fig. S4).

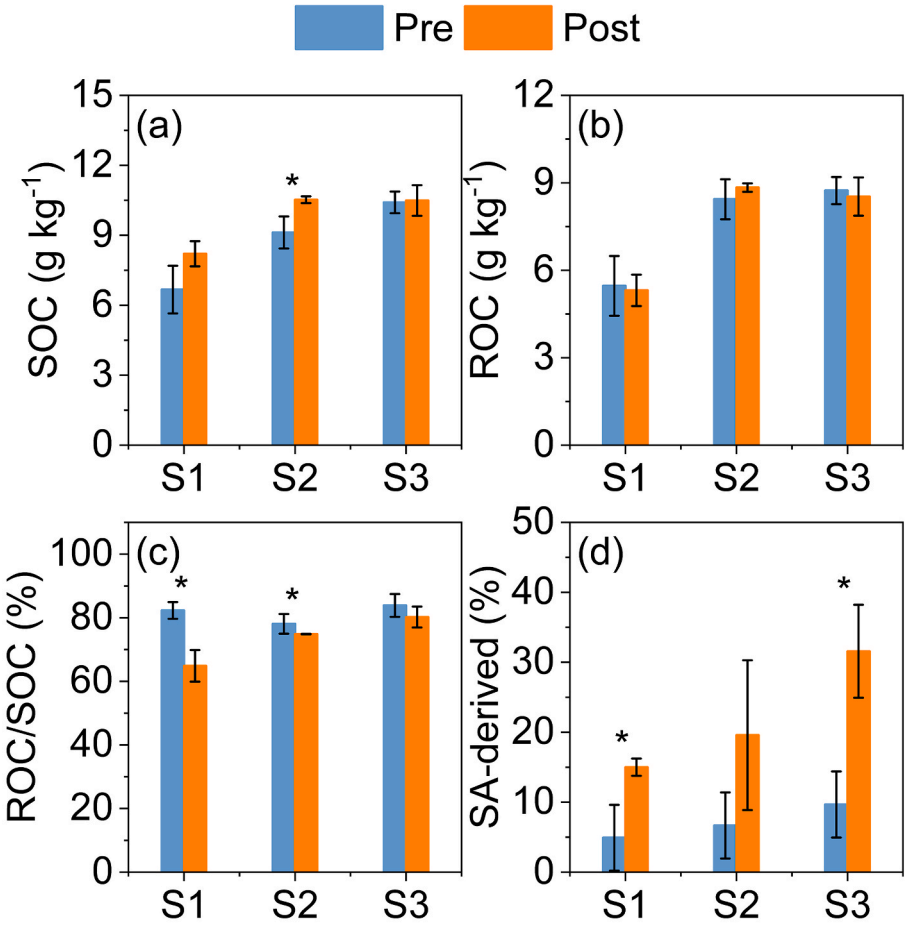


Fig. 1. Changes in sediment carbon components and their sources before and after *S. alterniflora* eradication. (a) Total sediment organic carbon (SOC); (b) Recalcitrant organic carbon (ROC); (c) Proportion of ROC in SOC; (d) Contribution of *S. alterniflora* to SOC. Column heights indicate as mean ± SE (standard error, n = 3). Asterisk above bars indicate significant differences among treatments ($p < 0.05$). Pre-eradication samples were collected in 2019 (S1), 2020 (S2), and 2022 (S3), while post-eradication samples were collected in 2023 at all stations.

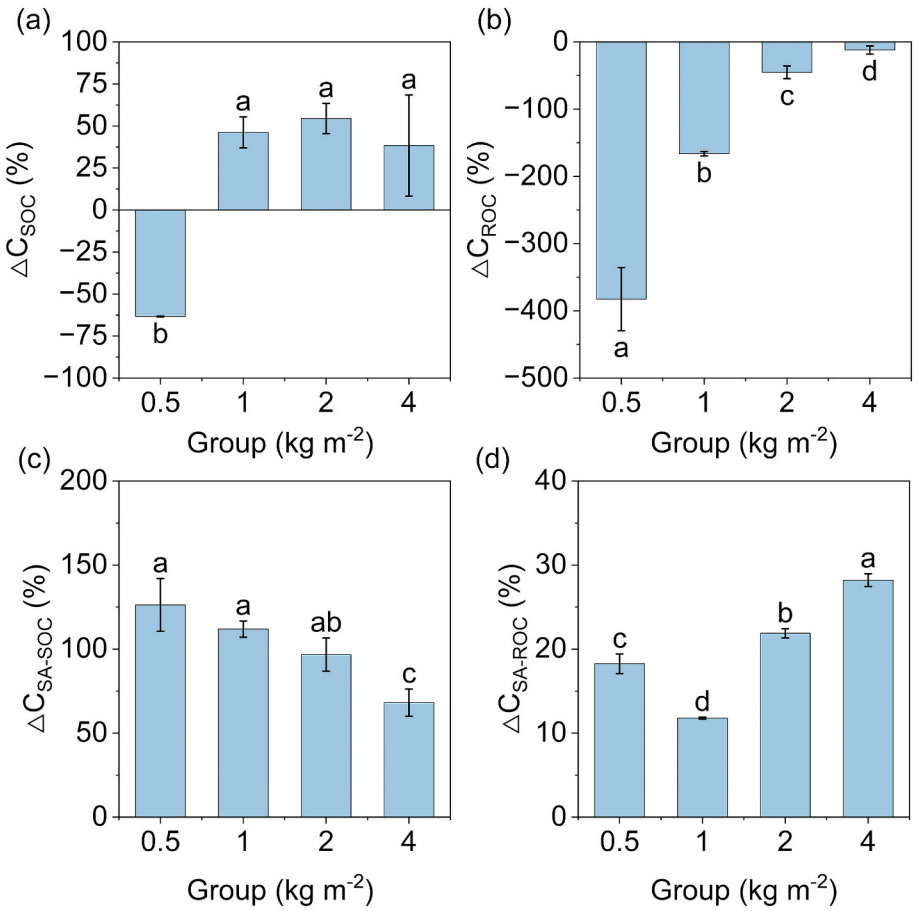


Fig. 2. Changes in SOC and ROC relative to CK versus different added doses of *S. alterniflora* residues. (a) Change in SOC relative to CK; (b) change in ROC relative to CK; (c) change in SOC derived from *S. alterniflora*; (d) change in ROC derived from *S. alterniflora*. Column heights indicate as mean ± SE (standard error). Lowercase letters above bars indicate significant differences among treatments ($p < 0.05$).

To characterize microbial genomes with predicted functions related to complex-carbon degradation, we examined the taxonomic composition of the recovered MAGs (Fig. 3e). Residue addition initially increased the abundances of Bacteroidota (bin.37, 40) and Pseudomonadota (bin.38-39). At the later stage, however, distinct dose-dependent enrichment patterns emerged. The H treatment was enriched in bin.1-bin.5, comprising Actinomycetota (bin.1), Bacteroidota (bin.2 and bin.5), Bacillota affiliated with Clostridia (bin.3), and Halobacteriota affiliated with Methanosarcinia (bin.4). Functionally, bin.2, bin.3, and bin.5 showed predicted genomic potential for cellulose, hemicellulose, and oligosaccharide degradation, whereas bin.1 and bin.4 were characterized mainly by amylolytic or chitin-associated enzyme markers. In contrast, the L treatment was enriched in Bacteroidota affiliated with Marinilabiliaceae (bin.6), Bacillota affiliated with Clostridia (bin.7 and bin.8), and Thermoproteota affiliated with Bathyarchaeia (bin.9). Notably, bin.6 exhibited the broadest predicted substrate-degradation repertoire among bin.1-bin.9, spanning cellulose, hemicellulose, oligosaccharide, starch, and chitin-associated functions. Bin.7 was associated mainly with hemicellulose and oligosaccharide degradation, whereas bin.8 and bin.9 showed predominantly amylolytic potential.

3.4. Microbial functions following residues addition

To compare the relative abundance of carbon-degrading functional genes across treatments, metagenomic clean reads were annotated against the CAZyme database. Following *S. alterniflora* residues addition, microbial communities showed higher relative abundances of specific CAZyme genes annotated for the degradation of plant-derived carbohydrates, including simpler sugar compounds (sucrose, beta-Fucosides, alpha-rhamnoside) and complex structural polysaccharides (starch, fructan, pectin, beta-galactan, arabinogalactan protein, beta-glucan, alpha-glucan, alpha-galactan, xyloglucan, xylan, arabinan, beta-glucuronan, cellulose and beta-mannan). In contrast, the relative abundance of genes responsible for degrading microbially derived complex polysaccharides decreased, such as peptidoglycan, chitin, and exopolysaccharides (Fig. 4a).

The genome-resolved MAG analysis provides predictions of the substrate-utilization potential of individual reconstructed genomes, whereas the CAZyme and KEGG analyses presented below characterize functional potential at the community level. These two approaches provide complementary information at different biological levels and are not intended for direct one-to-one comparison. KEGG pathway analysis further revealed differences in metabolic capacities between addition (L and H) and CK treatments (Fig. 4b). Residue addition enhanced flavone and flavonol biosynthesis, whereas carbon metabolism (e.g., fatty acid metabolism, glycerophospholipid metabolism, glyoxylate and dicarboxylate metabolism), degradation of plant secondary metabolites, and aromatic compound degradation were all reduced compared with the CK treatment, with stronger declines in the H treatment than in the L treatment.

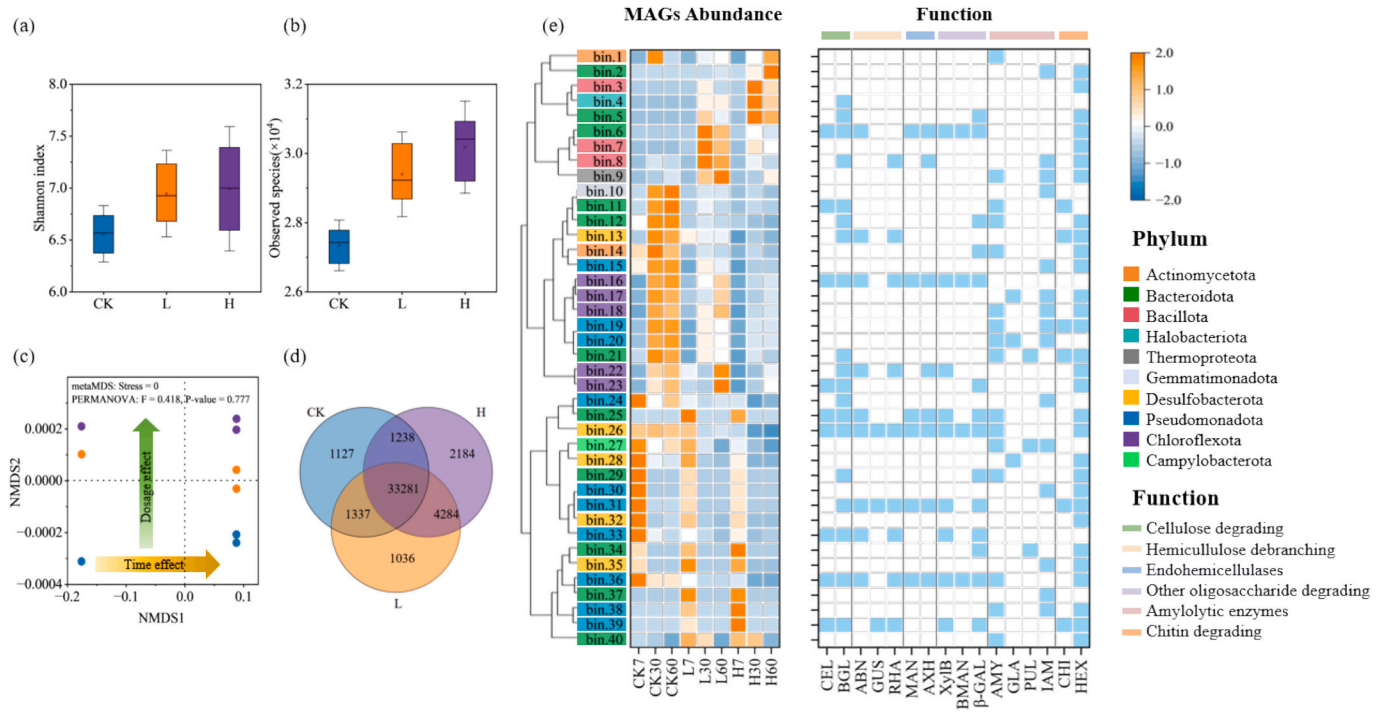


Fig. 3. Sediment microbial community composition following *S. alterniflora* residues addition. (a) Shannon index; (b) observed species; (c) non-metric multidimensional scaling (NMDS) plots; (d) Venn diagram; (e) Overview of 40 metagenome-assembled genomes (MAGs) involved in complex carbon degradation. Clustered based on the abundance of MAGs. The different taxonomic affiliations of the MAGs are indicated by distinct colors. The heatmap displays the abundance of these MAGs across different treatment groups (CK, L and H group), with high abundance represented in orange and low abundance in blue. The presence-absence map reveals specific complex carbon degradation functions corresponding to different MAGs, where the presence of genes filled in blue. The detailed descriptions of symbols, KEGG Orthology, etc., are provided in Table S3.

4. Discussion

4.1. Effect of S. Alterniflora residues addition on sediment organic carbon pools

The addition of *S. alterniflora* residues reduced the proportion of ROC, thereby reshaping the sediment carbon pool structure (Fig. 2a, b). ^{13}C isotope tracing revealed significant declines in ROC proportion (11–19% and 11–23% in field and laboratory experiments, respectively; Fig. 1, Fig. S3e). Contrary to the traditional view that ROC is highly resistant to microbial decomposition (Rovira and Vallejo, 2007, 2002; Zhang et al., 2017a), and that LOC inputs suppress ROC mineralization via negative PE (Liu et al., 2017; Zhang et al., 2017b), our findings indicate the opposite.

Microbial co-metabolism represents one plausible explanation for the loss of pre-existing ROC following residue addition. Residue inputs enhanced the community-level potential for utilization of plant-derived carbohydrates (Fig. 4a), consistent with increased availability of residue-derived substrates for microbial metabolism. The concurrent loss of pre-existing ROC is consistent with the possibility that metabolism supported by residue-derived substrates also affected native sediment carbon. Although the *S. alterniflora*-derived carbon partially replaced the mineralized ROC pool, this substitution reduced the chemical stability of sedimentary organic carbon pool. Because metagenomic annotations represent predicted functional potential rather than in situ activity, and neither ROC-specific enzyme activities nor isotope-resolved ROC mineralization were measured, these microbial interpretations should be regarded as mechanistic hypotheses supported by correlative metagenomic evidence rather than directly demonstrated pathways.

Exogenous carbon input exhibited a nonlinear relationship with ROC loss, whereby low-dose additions induced disproportionately greater losses (Fig. 2). To account for differences in residue input among treatments and to exclude the potential artifact of carbon dilution, ROC changes were normalized to the amount of *S. alterniflora* carbon added in each treatment (Fig. 2b). In addition, we further assumed that residues in the low-dose treatment (0.5 kg m^{-2}) contained no ROC. Under this extreme assumption, physical dilution would account for at most a ~ 4 % decline in the ROC/SOC ratio—substantially lower than the ~ 20 % reduction observed in our experiment (Fig. S3e). These results are inconsistent with residue dilution alone and are instead consistent with a microbial contribution to the observed nonlinear ROC loss.

Previous studies similarly reported that low-dose straw additions stimulated SOC loss, whereas higher doses led to SOC gains or comparable levels to controls (Bastida et al., 2019; Liang et al., 2023). In our study, net SOC loss occurred only under the 0.5 kg m^{-2} treatment, although native carbon losses were observed across all treatments, with a priming-like response under low-dose treatments (Fig. 2a). Notably, the 0.5 kg m^{-2} treatment also exhibited the greatest decline in ROC, highlighting its disproportionate vulnerability to residues addition. Moreover, low-dose addition caused net MBC loss (Fig. S7), indicating that while some microbes benefitted, others declined or underwent community restructuring. In the field survey, we did not detect a net loss of SOC after *S. alterniflora* eradication. This discrepancy with the incubation results may be explained by the rarity of extremely low residues inputs under natural conditions. Previous studies reported that the total biomass of *S. alterniflora* along the Chinese coastal wetlands ranges from 0.93 to 6.98 kg m^{-2} (Chen et al., 2024). Even when aboveground biomass is strictly prevented from entering sediments, only about 18% of invaded areas exhibit belowground biomass lower than 0.5 kg m^{-2}. Therefore, the low-dose scenarios that caused the most pronounced ROC loss in our incubation experiment are unlikely to dominate in the field, which may partly explain the absence of detectable SOC depletion at the ecosystem scale.

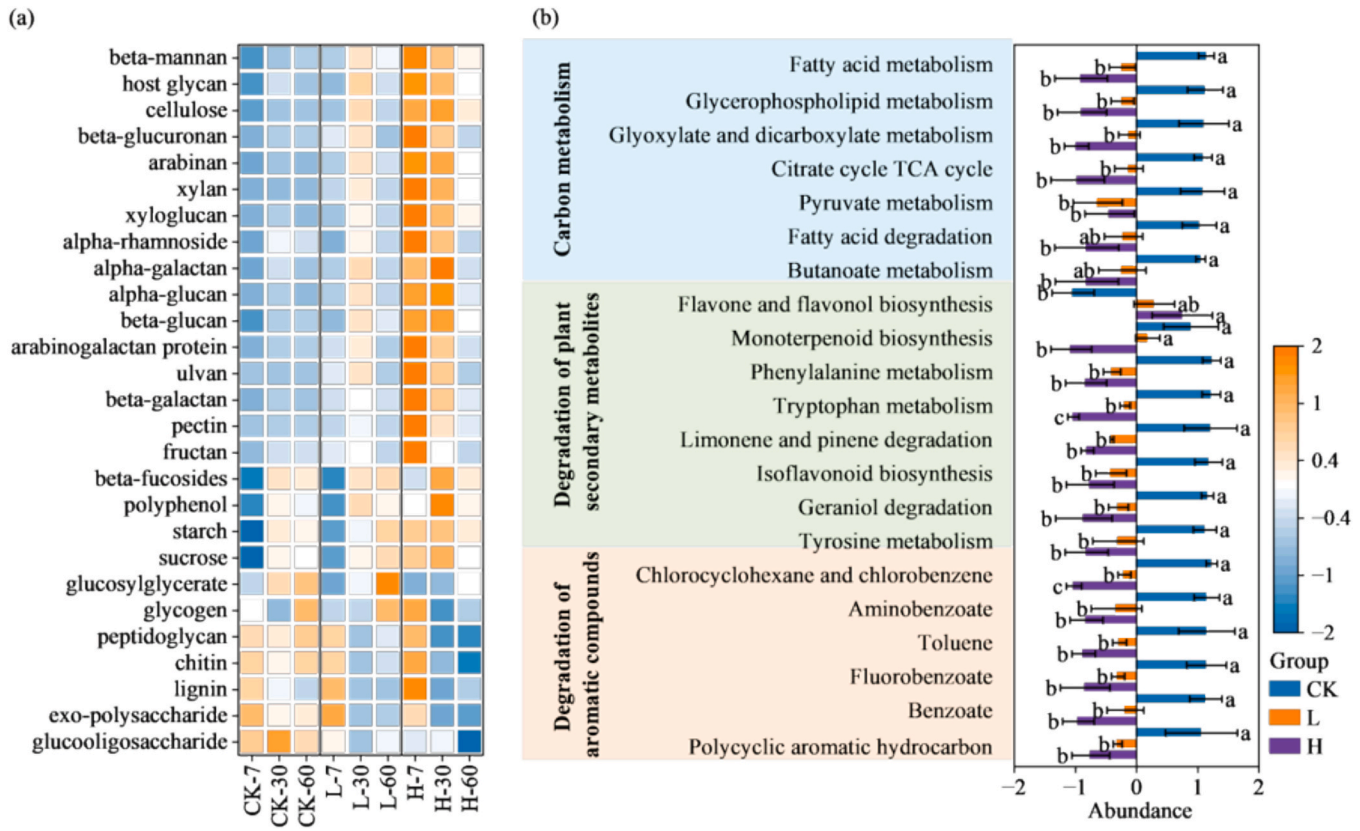


Fig. 4. Substrate utilization and functional pathways of microbial communities following *S. alterniflora* residues addition. (a) Heatmap of substrate utilization in CK (control, 0 kg m^{-2}), L (low dose addition, 1 kg m^{-2}), and H treatments (high dose addition, 4 kg m^{-2}) when day 7, 30 and 60; (b) Bar plots of normalized abundances of significantly enriched metabolic pathways.

4.2. Microbial community and functional shifts driving carbon processes after S. Alterniflora residues addition

In line with the 'co-metabolism' and 'nutrient mining' frameworks (Fang et al., 2018), limited labile carbon inputs were rapidly exploited by r-strategist microbes to support growth and extracellular enzyme production. Under carbon- and nutrient-limited conditions, microbes secreted more enzymes to mine native SOC. By contrast, high-dose additions fulfilled microbial carbon and energy demands, reducing the incentive to exploit recalcitrant SOC and channeling more carbon into microbial biomass. In our study, the overall microbial abundance and diversity were lower in the low-addition group compared to the high-addition group. However, the low-addition group was enriched in MAGs with broader predicted capacities for complex-carbon utilization. We refer to this pattern here as "active foraging", operationally defined as a microbial resource-acquisition response under limited residue supply characterized by enrichment of microorganisms with broader predicted capacities for utilizing complex carbon substrates.

Microbial community abundance and structure are key determinants of organic matter mineralization under labile carbon inputs (Garcia-Pausas and Paterson, 2011). Our results revealed clear community shifts following residues addition. In the early stage, both low (L) and high (H) treatments were enriched in r-strategist taxa, including Pseudomonadota (formerly Proteobacteria), Campylobacterota, and Bacteroidota (Fig. 3e, S3a). These copiotrophic groups thrive in nutrient-rich conditions and rapidly utilize DOC released during initial residues decomposition (Glasl et al., 2020; van der Stel and Wösten, 2019; Yao et al., 2017). Notably, Bacteroidota specialize in hemicellulose degradation (Huang et al., 2023), a major constituent of *S. alterniflora* (Yan et al., 2018). Moreover, the enrichment of Thermodesulfobacteriota may reflect greater potential for sulfate-associated carbon mineralization (Demin et al., 2024; Wang et al., 2025b). The sulfide (HS^-) generated during this process may disrupt iron-organic matter complexes (Fe-OC) through reductive dissolution, thereby releasing mineral-protected ROC and increasing its microbial availability (Melton et al., 2014). At this stage, compared with the H treatment, the abundance of r-strategist microorganisms was lower in the L treatment, whereas K-strategists such as Gemmatimonadota and Chloroflexota were more enriched (Fig. S4). This compositional shift is consistent with stronger selection for taxa adapted to resource-limited conditions under lower residue input, but does not demonstrate direct utilization of native ROC.

At day 30, the bacterial communities shifted toward dominance by Chloroflexota (Fig. S4a), although their overall abundance in the addition treatments was lower than in CK (Fig. 3e), with higher abundance in the L treatment compared to the H treatment. As typical K-strategists, Chloroflexota thrive on recalcitrant substrates such as cellulose and lignin (Yang et al., 2023). Concurrently, Bacillota (formerly Firmicutes) and Fibrobacterota increased in relative abundance compared with CK, whereas Actinobacteria, Acidobacteriota, and Gemmatimonadetes declined (Fig. 3e). Bacillota are metabolically versatile under nutrient-rich conditions (Dias et al., 2025), and Bacillus species are known lignin degraders (Fig. S4, Table S4; Grgas et al., 2023). Fibrobacterota specialize in efficient cellulose degradation (Neumann et al., 2018; Ransom-Jones et al., 2012). Actinobacteria are highly competitive in utilizing plant-derived DOC such as sugars and amino acids (Su et al., 2020) and are also key lignin degraders (Saini et al., 2015; Weng et al., 2021). Gemmatimonadetes possess GHs gene clusters that confer advantages in degrading lignin and hemicellulose (Bao et al., 2025). Collectively, these shifts indicate that the rapid mineralization capacity of r-strategist microbes diminished at later stages, while the long-term decomposition potential also declined, with enhanced activity

restricted to specific plant-derived substrates relative to CK. Moreover, the consistently higher abundance of K-strategist microbes in the low-dose addition treatments compared to the high-dose treatments suggests that limited labile carbon inputs favored microbial groups specialized in the efficient utilization of ROC pools.

Bacteria preferentially metabolize simple substrates to form amino sugars, whereas fungi target complex compounds (Zhang et al., 2025). The enrichment of Ascomycota may reflect increased potential for transformation of structurally complex organic matter, although their direct contribution to ROC degradation was not determined. Conversely, the decline of Basidiomycota in the H treatment indicates reduced humification potential and impaired stabilization of newly formed carbon. Bacteria preferentially degrade lighter carbon, whereas archaea can metabolize heavier carbon (Yang et al., 2024). Among archaea, Euryarchaeota increased in the addition treatments (Fig. S4c), consistent with our previous observations of *Methanomassiliicoccus* and *Methanosarcina*, which can contribute to lignin decomposition coupled with methane production (Liu et al., 2025b). Overall, residues addition promoted degraders of both labile and recalcitrant carbon while potentially hindering new carbon stabilization, creating a 'strong degradation, weak formation' scenario and preventing recovery of the carbon pool. Although we observed changes in the abundance of these archaeal and fungal groups, their exact contributions to ROC degradation or the formation and stabilization of new carbon require further validation through isolation and cultivation experiments or isotope-tracing approaches.

We demonstrated pronounced shifts in microbial functions following residues addition. Enhanced organic carbon mineralization indicated that the expanded microbial community primarily exploited the added *S. alterniflora* residues as substrates. Supporting evidence came from CAZyme annotation, which revealed significant enrichment of genes for degrading a broad spectrum of plant-derived polysaccharides (from arabinans to xylans and cellulose), as well as recalcitrant lignin (Fig. 4a; Fig. S6). This pattern suggests that *S. alterniflora* inputs promoted microbial consumption of plant-derived substrates (residues and native ROC) while suppressing utilization of microbially derived, inert substrates. In contrast, KEGG annotation showed reduced abundances of genes related to carbon metabolism and degradation of microbial extracellular polymers (e.g., chitin) (Fig. 4b), implying that microbes redirected resources toward residues exploitation rather than structural or stable product synthesis. This is consistent with the 'energy prioritized for external attack' hypothesis (Bastida et al., 2019).

4.3. Environmental implications and limitations

This study reveals that residues inputs from the eradication of *S. alterniflora* reshape sediment carbon pools and microbial processes in coastal wetlands. Residue addition reduced both the content and proportion of ROC, thereby weakening the stability of the SOC pool. Microbial responses played a central role, as communities shifted toward taxa specialized in degrading plant-derived substrates such as sugars, cellulose, hemicellulose, and lignin. Importantly, the relationship between residue dose and ROC loss was nonlinear: low inputs caused greater ROC depletion, whereas high inputs mitigated this effect. These findings suggest that management strategies should avoid small, scattered residue inputs that disproportionately accelerate ROC loss.

Our research also has its limitations. Firstly, the controlled incubation simplified several aspects of field conditions. Finely grinding the *S. alterniflora* residues increased their surface area and likely enhanced substrate accessibility, potentially accelerating decomposition relative to intact residues in the field. Similarly, slurry preparation disrupted the natural sediment structure and increased contact between residues, microorganisms, and sediment organic matter, which may have enhanced microbial activity and carbon accessibility. Therefore, the magnitude of ROC loss observed in the incubation should be interpreted as a potential response under highly mixed conditions rather than a direct estimate of field-scale carbon loss. An additional limitation concerns the operational definition of ROC used in this study. Although acid hydrolysis is widely used to isolate a chemically resistant fraction of SOC, the remaining carbon pool may still contain microbial necromass, mineral-associated organic carbon, and other compounds resistant to acid hydrolysis. Therefore, the acid-hydrolysis-defined ROC examined here should not be interpreted as equivalent to chemically inert or permanently stable carbon. Future studies combining chemical fractionation with biomarker, mineral-association, or isotope-based approaches would help better resolve the composition and persistence of this operationally defined ROC pool. The constant 30 °C incubation represented summer field conditions but did not capture seasonal temperature variability. Temperature fluctuations in natural wetlands may alter microbial activity, residue decomposition, and the magnitude of residue-induced native carbon loss, potentially modifying the observed dose–response relationship. In addition, the 60-day incubation captured only the early to intermediate stages of residue decomposition. As labile residue-derived substrates become depleted over longer periods, microbial substrate use and ROC vulnerability may change. Therefore, the lower relative ROC loss observed under high residue input should be interpreted as a short-term response rather than evidence of long-term protection of the ROC pool.

Secondly, scenarios involving repeated plant debris input due to the potential recurrence of *S. alterniflora* were excluded from the analysis. Consequently, a more thorough, life-cycle-based carbon footprint evaluation of plant residue management following *S. alterniflora* eradication is warranted in future research.

In addition to microbially mediated carbon loss, *S. alterniflora* eradication may also enhance physical sediment carbon loss. Salt-marsh vegetation attenuates hydrodynamic energy and stabilizes sediments through dense aboveground biomass and root systems, whereas vegetation removal may increase sediment resuspension and erosion. Such erosion may directly export SOC and expose previously protected carbon to further microbial decomposition, potentially coupling physical carbon loss with ROC destabilization. Although erosion was not quantified in this study, post-eradication carbon loss should therefore be considered as a combination of microbial decomposition and physical sediment redistribution, and erosion risk should also be considered in restoration management.

CRediT authorship contribution statement

Hui Wu: Writing – review & editing, Writing – original draft, Visualization, Methodology, Investigation, Formal analysis, Data curation, Conceptualization. **Meiqing Lu:** Formal analysis, Data curation. **Dan Yu:** Writing – review & editing, Validation. **Wenhong Xu:** Writing – review & editing, Methodology, Investigation. **Mengru Li:** Writing – review & editing, Methodology, Investigation. **Shiyao Chen:** Writing – review & editing, Methodology, Investigation, Conceptualization. **Zeyang Lu:** Writing – review & editing, Investigation. **Fenfang Wang:** Writing – review & editing, Methodology. **Nengwang Chen:** Writing – review & editing, Validation, Methodology, Funding acquisition, Conceptualization.

Declaration of competing interest

The authors declare that they have no known competing financial interests or personal relationships that could have appeared to influence the work reported in this paper.

Acknowledgments

This work was supported by the National Key R&D Program of China (2022YFF0802102); the National Natural Science Foundation of China (422706011); and the Shenzhen Science and Technology Plan Project (KCXST20221021111404011); MEL Internal Program (No.

MELRI2501). We are grateful to Wenyan Tang, Qibiao Yu, Huwei Li, Chunyan Cheng, and Yuyang Zheng for their help in field measurement, to Shaorong Fang from Information and Network Center of Xiamen University for the help with the high-performance computing, and to Junou Du and Fang Wu for their supportive technician work.

Appendix A. Supplementary data

Supplementary data to this article can be found online at https://doi.org/10.1016/j.geoderma.2026.118060.

Data availability

Data will be made available on request.

References

Alneberg, J., Bjarnason, B.S., de Bruijn, I., Schirmer, M., Quick, J., Ijaz, U.Z., Lahti, L., Loman, N.J., Andersson, A.F., Quince, C., 2014. Binning metagenomic contigs by coverage and composition. Nat. Methods 11, 1144–1146. https://doi.org/10.1038/nmeth.3103.

Alongi, D.M., 2022. Impacts of climate change on blue carbon stocks and fluxes in mangrove forests. Forests 13, 149. https://doi.org/10.3390/f13020149.

Bao, Y., Sáez-Sandino, T., Feng, Y., Yan, X., He, S., Feng, S., Chen, R., Guo, H., Delgado-Baquerizo, M., 2025. Gemmatirosa adaptations to arid and low soil organic carbon conditions worldwide. Geoderma 460, 117420. https://doi.org/10.1016/j.geoderma.2025.117420.

Bastida, F., García, C., Fierer, N., Eldridge, D.J., Bowker, M.A., Abades, S., Alfaro, F.D., Asefaw Berhe, A., Cutler, N.A., Gallardo, A., García-Velázquez, L., Hart, S.C., Hayes, P.E., Hernández, T., Hseu, Z.-Y., Jehmlich, N., Kirchmair, M., Lambers, H., Neuhauser, S., Peña-Ramírez, V.M., Pérez, C.A., Reed, S.C., Santos, F., Siebe, C., Sullivan, B.W., Trivedi, P., Vera, A., Williams, M.A., Luis Moreno, J., Delgado-Baquerizo, M., 2019. Global ecological predictors of the soil priming effect. Nat. Commun. 10, 3481. https://doi.org/10.1038/s41467-019-11472-7.

Bernard, L., Basile-Doelsch, I., Derrien, D., Fanin, N., Fontaine, S., Guenet, B., Karimi, B., Marsden, C., Maron, P., 2022. Advancing the mechanistic understanding of the priming effect on soil organic matter mineralisation. Funct. Ecol. 36, 1355–1377. https://doi.org/10.1111/1365-2435.14038.

Buchfink, B., Xie, C., Huson, D.H., 2015. Fast and sensitive protein alignment using DIAMOND. Nat. Methods 12, 59–60. https://doi.org/10.1038/nmeth.3176.

Chaumeil, P.-A., Mussig, A.J., Hugenholtz, P., Parks, D.H., 2020. GTDB-tk: A toolkit to classify genomes with the genome taxonomy database. Bioinformatics 36, 1925–1927. https://doi.org/10.1093/bioinformatics/btz848.

Chen, Y., Wu, F., Wang, Y., Guo, Y., Kirwan, M.L., Liu, W., Zhang, Y., 2024. Latitudinal trends in the biomass allocation of invasive *Spartina alterniflora*: implications for salt marsh adaptation to climate warming. Front. Mar. Sci. 11, 1510854. https://doi.org/10.3389/fmars.2024.1510854.

Cheng, L., Leavitt, S.W., Kimball, B.A., Pinter, P.J., Ottman, M.J., Matthias, A., Wall, G. W., Brooks, T., Williams, D.G., Thompson, T.L., 2007. Dynamics of labile and recalcitrant soil carbon pools in a sorghum free-air CO_2 enrichment (FACE) agroecosystem. Soil Biol. Biochem. 39, 2250–2263. https://doi.org/10.1016/j.soilbio.2007.03.031.

Chklovski, A., Parks, D.H., Woodcroft, B.J., Tyson, G.W., 2023. CheckM2: A rapid, scalable and accurate tool for assessing microbial genome quality using machine learning. Nat. Methods 20, 1203–1212. https://doi.org/10.1038/s41592-023-01940-w.

Craig, M.E., Geyer, K.M., Beidler, K.V., Brzostek, E.R., Frey, S.D., Stuart Grandy, A., Liang, C., Phillips, R.P., 2022. Fast-decaying plant litter enhances soil carbon in temperate forests but not through microbial physiological traits. Nat. Commun. 13, 1229. https://doi.org/10.1038/s41467-022-28715-9.

Demin, K.A., Prazdnova, E.V., Minkina, T.M., Gorovtsov, A.V., 2024. Sulfate-reducing bacteria unearthed: Ecological functions of the diverse prokaryotic group in terrestrial environments. Appl. Environ. Microbiol. https://doi.org/10.1128/aem.01390-23.

Dias, B., do, C., Lamarca, A.P., Machado, D.T., Kloh, V.P., de Carvalho, F.M., Vasconcelos, A.T.R., 2025. Metabolic pathways associated with firmicutes prevalence in the gut of multiple livestock animals and humans. Anim. Microbiome 7, 20. https://doi.org/10.1186/s42523-025-00379-y.

Fan, Y., Zhou, Z., Liu, F., Qian, L., Yu, X., Huang, F., Hu, R., Su, H., Gu, H., Yan, Q., He, Z., Wang, C., 2024. The vertical partitioning between denitrification and dissimilatory nitrate reduction to ammonium of coastal mangrove sediment microbiomes. Water Res. 262, 122113. https://doi.org/10.1016/j.watres.2024.122113.

Fang, Y., Nazaries, L., Singh, B.K., Singh, B.P., 2018. Microbial mechanisms of carbon priming effects revealed during the interaction of crop residue and nutrient inputs in contrasting soils. Glob. Chang. Biol. 24, 2775–2790. https://doi.org/10.1111/gcb.14154.

Fontaine, S., Barot, S., Barré, P., Bdioui, N., Mary, B., Rumpel, C., 2007. Stability of organic carbon in deep soil layers controlled by fresh carbon supply. Nature 450, 277–280. https://doi.org/10.1038/nature06275.

Gao, G.F., Li, P.F., Shen, Z.J., Qin, Y.Y., Zhang, X.M., Ghoto, K., Zhu, X.Y., Zheng, H.L., 2018. Exotic *Spartina alterniflora* invasion increases CH_4 while reduces CO_2 emissions from mangrove wetland soils in southeastern China. Sci. Rep. 8, 9243. https://doi.org/10.1038/s41598-018-27625-5.

Garcia-Pausas, J., Paterson, E., 2011. Microbial community abundance and structure are determinants of soil organic matter mineralisation in the presence of labile carbon. Soil Biol. Biochem. 43, 1705–1713. https://doi.org/10.1016/j.soilbio.2011.04.016.

Glasl, B., Robbins, S., Frade, P.R., Marangon, E., Laffy, P.W., Bourne, D.G., Webster, N.S., 2020. Comparative genome-centric analysis reveals seasonal variation in the function of coral reef microbiomes. ISME J. 14, 1435–1450. https://doi.org/10.1038/s41396-020-0622-6.

Grgas, D., Rukavina, M., Bešlo, D., Štefanac, T., Crnek, V., Šikić, T., Habuda-Stanić, M., Landeka Dragičević, T., 2023. The bacterial degradation of lignin—a review. Water 15, 1272. https://doi.org/10.3390/w15071272.

Huang, J., Gao, K., Yang, L., Lu, Y., 2023. Successional action of bacteroidota and firmicutes in decomposing straw polymers in a paddy soil. Environ. Microbiome. 18, 76. https://doi.org/10.1186/s40793-023-00533-6.

Huang, M., Zhang, Y., Zhou, Z., Zhu, X., 2022. A dataset of the UAV remote sensing spatial distribution of *Spartina alterniflora* in the Zhangjiang Estuary of Fujian Province from 2013 to 2022. https://doi.org/10.57760/SCIENCEDB.O00119.00069.

Hyatt, D., Chen, G.-L., LoCascio, P.F., Land, M.L., Larimer, F.W., Hauser, L.J., 2010. Prodigal: Prokaryotic gene recognition and translation initiation site identification. BMC Bioinformatics 11, 119. https://doi.org/10.1186/1471-2105-11-119.

Jian, J., Du, X., Reiter, M.S., Stewart, R.D., 2020. A meta-analysis of global cropland soil carbon changes due to cover cropping. Soil Biol. Biochem. 143, 107735. https://doi.org/10.1016/j.soilbio.2020.107735.

Kang, D.D., Li, F., Kirton, E., Thomas, A., Egan, R., An, H., Wang, Z., 2019. MetaBAT 2: An adaptive binning algorithm for robust and efficient genome reconstruction from metagenome assemblies. Peerj 7, e7359. https://doi.org/10.7717/peerj.7359.

Kuzyakov, Y., 2010. Priming effects: Interactions between living and dead organic matter. Soil Biol. Biochem. 42, 1363–1371. https://doi.org/10.1016/j.soilbio.2010.04.003.

Kuzyakov, Y., Friedel, J.K., Stahr, K., 2000. Review of mechanisms and quantification of priming effects. Soil Biol. Biochem. 32, 1485–1498. https://doi.org/10.1016/S0038-0717(00)00084-5.

Li, D., Liu, C.-M., Luo, R., Sadakane, K., Lam, T.-W., 2015. MEGAHIT: An ultra-fast single-node solution for large and complex metagenomics assembly via succinct *de bruijn* graph. Bioinformatics 31, 1674–1676. https://doi.org/10.1093/bioinformatics/btv033.

Li, H., Mao, D., Wang, Z., Huang, X., Li, L., Jia, M., 2022a. Invasion of *Spartina alterniflora* in the coastal zone of mainland China: Control achievements from 2015 to 2020 towards the Sustainable Development Goals. J. Environ. Manage. 8.549 323, 116242. https://doi.org/10.1016/j.jenvman.2022.116242.

Li, J., Han, G., Wang, G., Liu, X., Zhang, Q., Chen, Y., Song, W., Qu, W., Chu, X., Li, P., 2022b. Imbalanced nitrogen–phosphorus input alters soil organic carbon storage and mineralisation in a salt marsh. CATENA 208, 105720. https://doi.org/10.1016/j.catena.2021.105720.

Li, R., Yu, C., Li, Y., Lam, T.-W., Yiu, S.-M., Kristiansen, K., Wang, J., 2009. SOAP2: An improved ultrafast tool for short read alignment. Bioinformatics 25, 1966–1967. https://doi.org/10.1093/bioinformatics/btp336.

Li, S., Lyu, M., Deng, C., Deng, W., Wang, X., Cao, A., Jiang, Y., Liu, J., Lu, Y., Xie, J., 2024. Input of high-quality litter reduces soil carbon losses due to priming in a subtropical pine forest. Soil Biol. Biochem. 194, 109444. https://doi.org/10.1016/j.soilbio.2024.109444.

Liang, Z., Rasmussen, J., Poeplau, C., Elsgaard, L., 2023. Priming effects decrease with the quantity of cover crop residues – potential implications for soil carbon sequestration. Soil Biol. Biochem. 184, 109110. https://doi.org/10.1016/j.soilbio.2023.109110.

Liu, C., Li, L., He, C., Zhang, G., Liu, X., Liu, C., Zhang, Y., Li, P., Zhang, Y., Zhang, L., 2025a. Divergent accumulations of microbial-derived carbon and iron-bound organic carbon in mangrove soil organic matter fractions along a salinity gradien. CATENA 260, 109457. https://doi.org/10.1016/j.catena.2025.109457.

Liu, T., Li, L., Xue, K., Wang, X., Li, H., Wang, Y., Dong, X., 2025b. Methane production from lignin in anoxic peatland. Nat. Geosci. 1–8. https://doi.org/10.1038/s41561-025-01758-5.

Liu, X.-J.-A., Sun, J., Mau, R.L., Finley, B.K., Compson, Z.G., Van Gestel, N., Brown, J.R., Schwartz, E., Dijkstra, P., Hungate, B.A., 2017. Labile carbon input determines the direction and magnitude of the priming effect. Appl. Soil Ecol. 109, 7–13. https://doi.org/10.1016/j.apsoil.2016.10.002.

Lu, Z., Xiao, K., Wang, F., Wang, Y., Yu, Q., Chen, N., 2023. Salt marsh invasion reduces recalcitrant organic carbon pool while increases lateral export of dissolved inorganic carbon in a subtropical mangrove wetland. Geoderma, No 437, 116573. https://doi.org/10.1016/j.geoderma.2023.116573.

Macreadie, P.I., Costa, M.D.P., Atwood, T.B., Friess, D.A., Kelleway, J.J., Kennedy, H., Lovelock, C.E., Serrano, O., Duarte, C.M., 2021. Blue carbon as a natural climate solution. Nat. Rev. Earth Environ. 2, 826–839. https://doi.org/10.1038/s43017-021-00224-1.

Mao, D., Liu, M., Wang, Z., Li, L., Man, W., Jia, M., Zhang, Y., 2019. Rapid invasion of *Spartina alterniflora* in the coastal zone of mainland China: Spatiotemporal patterns and human prevention. Sensors (basel) 19, 2308. https://doi.org/10.3390/s19102308.

Martin, M., 2011. Cutadapt removes adapter sequences from high-throughput sequencing reads. Embnet J. 17, 10. https://doi.org/10.14806/ej.17.1.200.

Melton, E.D., Swanner, E.D., Behrens, S., Schmidt, C., Kappler, A., 2014. The interplay of microbially mediated and abiotic reactions in the biogeochemical fe cycle. Nat. Rev. Microbiol. 12, 797–808. https://doi.org/10.1038/nrmicro3347.

Mendoza, O., De Neve, S., Deroo, H., Li, H., Sleutel, S., 2022. Do interactions between application rate and native soil organic matter content determine the degradation of exogenous organic carbon? Soil Biol. Biochem. 164, 108473. https://doi.org/10.1016/j.soilbio.2021.108473.

Neumann, A.P., Weimer, P.J., Suen, G., 2018. A global analysis of gene expression in fibrobacter succinogenes S85 grown on cellulose and soluble sugars at different growth rates. Biotechnol Biofuels 11, 295. https://doi.org/10.1186/s13068-018-1290-x.

Olm, M.R., Brown, C.T., Brooks, B., Banfield, J.F., 2017. dRep: A tool for fast and accurate genomic comparisons that enables improved genome recovery from metagenomes through de-replication. ISME J. 11, 2864–2868. https://doi.org/10.1038/ismej.2017.126.

Paterson, E., Sim, A., 2013. Soil-specific response functions of organic matter mineralization to the availability of labile carbon. Global Change Biol. 19, 1562–1571. https://doi.org/10.1111/gcb.12140.

Qi, G., Li, L., Li, H., Liu, Y., Xie, T., Guo, H., Ma, Z., Wu, J., Li, B., Ma, J., 2024. Ecological effects of the huge invasive species removal project in coastal China. Environ. Sci. Technol. 58, 21229–21241. https://doi.org/10.1021/acs.est.4c05253.

Ransom-Jones, E., Jones, D.L., McCarthy, A.J., McDonald, J.E., 2012. The fibrobacteres: An important phylum of cellulose-degrading bacteria. Microb. Ecol. 63, 267–281. https://doi.org/10.1007/s00248-011-9998-1.

Rovira, P., Vallejo, V.R., 2007. Labile, recalcitrant, and inert organic matter in mediterranean forest soils. Soil Biol. Biochem. 39, 202–215. https://doi.org/10.1016/j.soilbio.2006.07.021.

Rovira, P., Vallejo, V.R., 2002. Labile and recalcitrant pools of carbon and nitrogen in organic matter decomposing at different depths in soil: An acid hydrolysis approach. Geoderma 107, 109–141. https://doi.org/10.1016/S0016-7061(01)00143-4.

Saini, A., Aggarwal, N.K., Sharma, A., Yadav, A., 2015. Actinomycetes: A source of Lignocellulolytic Enzymes. Enzyme Research 2015, 1–15. https://doi.org/10.1155/2015/279381.

Sauvadet, M., Lashermes, G., Alavoine, G., Recous, S., Chauvat, M., Maron, P.-A., Bertrand, I., 2018. High carbon use efficiency and low priming effect promote soil C stabilization under reduced tillage. Soil Biol. Biochem. 123, 64–73. https://doi.org/10.1016/j.soilbio.2018.04.026.

Song, X., Wang, Y., Mei, B., Zhang, X., Zheng, P., Song, W., Tian, B., Qiqige, H.G., Xie, B., 2024. Effects of *Spartina alterniflora* control on soil carbon and nitrogen in coastal wetlands. Watershed Ecology Environ. 6, 54–62. https://doi.org/10.1016/j.wsee.2024.03.002.

Steinegger, M., Söding, J., 2017. MMseqs2 enables sensitive protein sequence searching for the analysis of massive data sets. Nat. Biotechnol. 35, 1026–1028. https://doi.org/10.1038/nbt.3988.

Su, Y., He, Z., Yang, Y., Jia, S., Yu, M., Chen, X., Shen, A., 2020. Linking soil microbial community dynamics to straw-carbon distribution in soil organic carbon. Sci. Rep. 10, 5526. https://doi.org/10.1038/s41598-020-62198-2.

Sun, S., Song, Z., Chen, B., Wang, Y., Ran, X., Fang, Y., Van Zwieten, L., Hartley, I.P., Wang, Y., Li, Q., Wu, L., Liu, C.-Q., Wang, H., 2023. Current and future potential soil organic carbon stocks of vegetated coastal ecosystems and their controls in the Bohai Rim Region. China. CATENA 225, 107023. https://doi.org/10.1016/j.catena.2023.107023.

Uritskiy, G.V., DiRuggiero, J., Taylor, J., 2018. MetaWRAP—a flexible pipeline for genome-resolved metagenomic data analysis. Microbiome 6, 158. https://doi.org/10.1186/s40168-018-0541-1.

van der Stel, A.-X., Wösten, M.M.S.M., 2019. Regulation of respiratory pathways in campylobacterota: A review. Front. Microbiol. 10. https://doi.org/10.3389/fmicb.2019.01719.

Wang, D., Labra, F.A., Yang, H., Hu, Y., Zhao, Z., Zhou, W., Yuan, L., 2025a. Restoration of native saltmarshes enhances carbon sequestration and mitigates warming effects following *Spartina alterniflora* removal. J. Appl. Ecol. 62, 2005–2017. https://doi.org/10.1111/1365-2664.70096.

Wang, H., Du, Q., Wang, Y., Xu, H., Wei, Z., Wang, X., 2024. GPro: Generative AI-empowered toolkit for promoter design. Bioinformatics 40, btae123. https://doi.org/10.1093/bioinformatics/btae123.

Wang, H., Zhong, Y., Yang, Q., Li, J., Li, D., Wu, J., Yang, S., Liu, J., Deng, Y., Song, J., Peng, P., 2025b. Coupling of sulfate reduction and dissolved organic carbon degradation accelerated by microplastics in blue carbon ecosystems. Water Res. 279, 123414. https://doi.org/10.1016/j.watres.2025.123414.

Weng, C., Peng, X., Han, Y., 2021. Depolymerization and conversion of lignin to value-added bioproducts by microbial and enzymatic catalysis. Biotechnol Biofuels 14, 84. https://doi.org/10.1186/s13068-021-01934-w.

Wu, H., Chen, Y., Chen, S., Li, M., Zhang, Y., Zhao, M., Han, G., Chen, N., 2026. Hydrological inundation threshold regulates the carbon source-sink transition in unvegetated tidal flats. Water Res. 305, 126544. https://doi.org/10.1016/j.watres.2026.126544.

Wu, Y.-W., Simmons, B.A., Singer, S.W., 2016. MaxBin 2.0: An automated binning algorithm to recover genomes from multiple metagenomic datasets. Bioinformatics 32, 605–607. https://doi.org/10.1093/bioinformatics/btv638.

Xie, B., 2019. Resource utilization of invasive *Spartina alterniflora*: A review. Chin. J. Eco-Agric. 12, 1870–1879. https://doi.org/10.13930/j.cnki.cjea.190339.

Yan, J., Wang, L., Hu, Y., Tsang, Y.F., Zhang, Y., Wu, J., Fu, X., Sun, Y., 2018. Plant litter composition selects different soil microbial structures and in turn drives different litter decomposition pattern and soil carbon sequestration capability. Geoderma 319, 194–203. https://doi.org/10.1016/j.geoderma.2018.01.009.

Yang, M., Liu, N., Wang, B., Li, Y., Li, W., Shi, X., Yue, X., Liu, C.-Q., 2024. Stepwise degradation of organic matters driven by microbial interactions in China´s coastal wetlands: Evidence from carbon isotope analysis. Water Res. 250, 121062. https://doi.org/10.1016/j.watres.2023.121062.

Yang, W., Zhao, H., Chen, X., Yin, S., Cheng, X., An, S., 2013. Consequences of short-term C_4 plant *Spartina alterniflora* invasions for soil organic carbon dynamics in a coastal wetland of eastern China. Ecol. Eng. 61, 50–57. https://doi.org/10.1016/j.ecoleng.2013.09.056.

Yang, Y., Dou, Y., Wang, B., Xue, Z., Wang, Y., An, S., Chang, S.X., 2023. Deciphering Factors Driving Soil Microbial Life-History Strategies in Restored Grasslands. iMeta 2, e66. https://doi.org/10.1002/imt2.66.

Yao, F., Yang, S., Wang, Z., Wang, X., Ye, J., Wang, X., DeBruyn, J.M., Feng, X., Jiang, Y., Li, H., 2017. Microbial taxa distribution is associated with ecological trophic cascades along an elevation gradient. Front. Microbiol. 8. https://doi.org/10.3389/fmicb.2017.02071.

Yu, X., Wang, L., Wang, Q., Zhou, G., Sun, H., Guggenberger, G., Li, Y., Yakov, K., Luo, Y., Fu, Y., 2025. Faster soil organic carbon turnover in MAOM versus POM: Straw input causes larger microbial driven soil organic carbon decomposition but higher straw accumulation in MAOM. Soil till. Res. 251, 106549. https://doi.org/10.1016/j.still.2025.106549.

Zhang, J., Tang, X., Zhong, S., Yin, G., Gao, Y., He, X., 2017a. Recalcitrant carbon components in glomalin-related soil protein facilitate soil organic carbon preservation in tropical forests. Sci. Rep. 7, 2391. https://doi.org/10.1038/s41598-017-02486-6.

Zhang, J., Zhang, F., Yang, L., 2025. Differences in straw derived hydrophilic and hydrophobic carbon incorporation into soil microbial necromass. Soil Biol. Biochem. 209, 109901. https://doi.org/10.1016/j.soilbio.2025.109901.

Zhang, X., Han, X., Yu, W., Wang, P., Cheng, W., 2017b. Priming effects on labile and stable soil organic carbon decomposition: Pulse dynamics over two years. PLOS ONE 12, e0184978. https://doi.org/10.1371/journal.pone.0184978.

Zheng, J., Ge, Q., Yan, Y., Zhang, X., Huang, L., Yin, Y., 2023. dbCAN3: Automated carbohydrate-active enzyme and substrate annotation. Nucl. Acids Res. 51, W115–W121. https://doi.org/10.1093/nar/gkad328.

Zhou, Z., Tran, P.Q., Breister, A.M., Liu, Y., Kieft, K., Cowley, E.S., Karaoz, U., Anantharaman, K., 2022. METABOLIC: High-throughput profiling of microbial genomes for functional traits, metabolism, biogeochemistry, and community-scale functional networks. Microbiome 10, 33. https://doi.org/10.1186/s40168-021-01213-8.

Zhu, X., Ma, M., Li, L., Li, M., 2024. Impacts of intensive smooth cordgrass removal on net ecosystem exchange in a saltmarsh-mangrove ecotone of Southeast China. Sci. Total Environ. 934, 173202. https://doi.org/10.1016/j.scitotenv.2024.173202.

Zhu, X., Meng, L., Zhang, Y., Weng, Q., Morris, J., 2019. Tidal and meteorological influences on the growth of invasive *Spartina alterniflora*: Evidence from UAV remote sensing. Remote Sensing 11, 1208. https://doi.org/10.3390/rs11101208.

Zhu, X., Qin, Z., Liu, W., Kirwan, M.L., Lu, H., Lee, S.Y., Dai, M., 2025. Coastal restoration may not necessarily enhance blue carbon sink. Geophys. Res. Lett. 52, e2025GL114614. https://doi.org/10.1029/2025GL114614.